Nanoscale

Accepted Manuscript

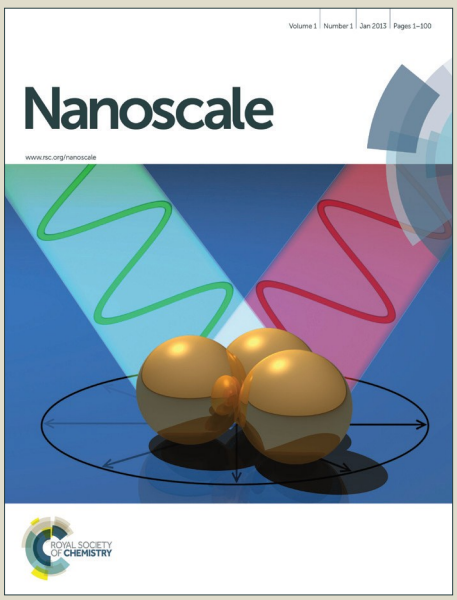

ROYAL SOCIETY OF CHEMISTRY

www.rsc.org/nanoscale

Journal Name

ARTICLE

Bandgap tunable colloidal Cu-based ternary and quaternary chalcogenide nanosheets *via* partial cation exchange

Received 00th January 20xx,
Accepted 00th January 20xx

DOI: 10.1039/x0xx00000x

www.rsc.org/

Parthiban Ramasamy,[a] Miri Kim,[b] Hyun-Soo Ra,[a] Jinkwon Kim,*[,b] and Jong-Soo Lee*[,a]

Copper based ternary and quaternary semiconductor nanostructures are of great interest for the fabrication of low cost photovoltaics. Although well-developed syntheses are available for zero dimensional (0D) nanoparticles, colloidal synthesis of two dimensional (2D) nanosheets remains a big challenge. Here we report, for the first time, a simple and reproducible cation exchange approach for 2D colloidal Cu_2GeSe_3, $Cu_2ZnGeSe_4$ and their alloyed $Cu_2GeS_xSe_{3-x}$, $Cu_2ZnGeS_xSe_{4-x}$ nanosheets using pre-synthesized $Cu_{2-x}Se$ nanosheets as template. Mechanism for the formation of $Cu_{2-x}Se$ nanosheets have been studied in detail. *In situ* oxidation of Cu^+ ions to form CuSe secondary phase facilitates the formation of $Cu_{2-x}Se$ NSs. The obtained ternary and quaternary nanosheets have average lateral size in micrometers and thickness less than 5 nm. This method is general and can be extended to produce other important ternary semiconductor nanosheets such as $CuIn_{1-x}Ga_xSe_2$. The optical band gap of these nanosheets is tuned from 1 to 1.48 eV, depending on their composition.

1. Introduction

The discovery of graphene has ignited global interest in the study of two-dimensional (2D) nanomaterials owing to their unique properties and potential application in photovoltaics, field effect transistors, batteries, and photodetectors.[1] The most extensively studied 2D nanomaterials are graphene and transition metal dichalcogenides (e.g. MoS_2, $MoSe_2$, WS_2 and WSe_2).[1-7] Most of their interesting properties are associated with their smaller thickness and 2D morphology. This inspires the exploration of other equally potential materials in 2D form for various applications.

One interesting family of materials are copper-based ternary (I_2-IV-VI_3) and quaternary (I-II-IV-VI_4) semiconductor nanocrystals. During the last years, they have gained a great deal of attention in the field of photovoltaic research as alternatives of CdTe and $Cu(In_{1-x}Ga_x)Se_2$ owing to their earth abundance, low toxicity, high absorption coefficients and compositionally tunable band gaps.[8-14] Besides photovoltaic applications, these multinary chalcogenide nanomaterials have been reported to show good thermoelectric properties due to their intrinsic lower thermal conductivities, which arises from the complex crystallographic structures.[15-17] Conventionally, colloidal ternary and quaternary nanocrystals have been prepared either by hot injection or one pot heating up methods.[8,18] The most commonly observed morphologies in these systems are 0D nanoparticles (NPs) and 1D nanorods (NRs).[8-14,19,20] A few reports on the synthesis of 2D nanoplates have also been reported.[21-23] However, the synthesis of micrometer sized 2D nanosheets (NSs) have rarely been reported for Cu-based multinary chalcogenides.[24] This is because of their non-layered crystal structures which do not have intrinsic driving force for 2D anisotropic growth. Recently, partial cation exchange (CE) methods have emerged as a powerful tool to control the composition in ternary and quaternary chalcogenides.[21-23,25-28] In the partial cation exchange methods, initial morphology of the nanocrystal template is retained and thus enable one to synthesize multinary chalcogenide nanomaterials with variety of morphologies which are not easily accessible by hot injection methods. One of the recent examples is the synthesis of luminescent $CuInSe_2/CuInS_2$ dot core/rod shell heterostructures from CdSe/CdS dot core/rod shell heterostructures by Donega and co-workers.[29]

Among the Cu-based multinary chalcogenides, $Cu_2ZnSnS(Se)_4$ nanocrystals are most extensively studied due to their earth abundant constituents and excellent photovoltaic properties.[30,31] Another potentially attractive but less explored materials are germanium containing Cu-based multinary chalcogenide nanocrystals such as Cu_2GeSe_3 (CGSe) and $Cu_2ZnGeSe_4$ (CZGSe). Both CGSe and CZGSe are reported experimentally and theoretically to be p-type semiconductor with direct band gap values between 0.78 and 1.63 eV.[32-35] This makes them ideal candidates for cadmium- and indium-free photovoltaic absorber materials. In addition, CGSe and

[a] Department of Energy Systems Engineering, DGIST, Daegu, 711-873, Republic of Korea. E-mail: jslee@dgist.ac.kr
[b] Department of chemistry and GETRC, Kongju National University, 182 shinkwon, Kongju, Chungnam, 314-701, Republic of Korea. E-mail: jkim@kongju.ac.kr

Electronic Supplementary Information (ESI) available: supporting information figures S1-S13. See DOI: 10.1039/x0xx00000x

CZGSe nanocrystals have been reported to exhibit good thermoelectric properties. A figure of merit of thermoelectric (ZT) up to 0.55 at 723 K has been reported for CZGSe nanocrystals.[15] The aforementioned issues together with the exciting properties of CGSe and CZGSe nanocrystals inspired us to develop new synthetic methods for these chalcogenides with tunable composition.

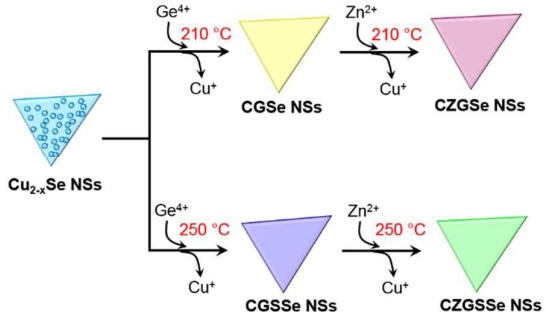

Fig. 1 Schematic of partial cation exchange synthesis of ternary and quaternary NSs from $Cu_{2-x}Se$ NSs.

Here we present a facile and reproducible approach for the synthesis of CGSe, CZGSe and their alloyed NSs *via* partial cation exchange (CE) with Ge^{4+} and Zn^{2+} ions, starting from $Cu_{2-x}Se$ NSs. The detailed synthetic scheme is shown in Fig. 1. Initially, $Cu_{2-x}Se$ NSs were synthesized using recently reported Se-precursor (selenium powder dissolved in oleylamine (OAm) and 1-dodecanethiol (1-DDT)).[36] In the second step, CGSe NSs were obtained by partially replacing Cu^{+} cations with Ge^{4+} cations at 210 °C. We also found that, sulfur can be alloyed with CGSe NSs to form $Cu_2GeS_xSe_{3-x}$ (CGSSe) by increasing CE reaction temperature to 250 °C. Finally, Zn^{2+} ions were incorporated to form quaternary CZGSe and alloyed $Cu_2ZnGeS_xSe_{4-x}$ (CZGSSe) NSs at 210 and 250 °C, respectively. The generality of our method is demonstrated by converting $Cu_{2-x}Se$ NSs to other important photovoltaic materials such as $CuInSe_2$, $CuIn_{1-x}Ga_xSe_2$ and $CuGaSe_2$. To best of our knowledge, a simple synthetic approach for the synthesis of 2D ternary and quaternary NSs has not been demonstrated previously. The synthesis method presented here will enable researchers to explore more conventional semiconductors in 2D morphology for photovoltaics and other optoelectronic applications.

2. Experimental

Materials and Methods:

Copper(I) iodide (CuI, 99.999%), germanium(IV) iodide (GeI_4, 99.99%), zinc(II) chloride ($ZnCl_2$, 99.999%), indium(III) chloride ($InCl_3$, 99.999), gallium(III) chloride ($GaCl_3$, 99.999%), selenium powder (Se, 99.99%), oleylamine (OAm, 70%), oleic acid (OA, 90%), 1-dodecanethiol (1-DDT, >98%), trioctylphosphine (TOP, 90%) were all used as received from Sigma Aldrich. Toluene (99.5%) was purchased from Alfa Aesar. Acetone and chloroform (HPLC grade) were purchased from Samchun chemicals, Korea.

Synthesis of $Cu_{2-x}Se$ NSs:

0.4 mmol CuI together with 10 mL of OAm and 4 mL of OA were loaded into a three-necked flask (50 mL) at room temperature. The mixture was degassed under vacuum with vigorous stirring at 150 °C for 1 h. The solution colour was changed from blue to clear yellow. The solution was then purged with nitrogen, and the Se precursor prepared by ultrasonication of 0.3 mmol of Se powder in a mixture of 0.5 mL OAm and 0.5 mL 1-DDT was quickly injected into the resulting solution at 150 °C. This produced a colour change from yellow to dark green. After stirring at 150 °C for 2 h, the mixture was cooled to room temperature. This mixture containing $Cu_{2-x}Se$ NSs (denoted as **solution 1**) was directly used for further growth of ternary or quaternary chalcogenide NSs, which will be described in the following paragraphs. For characterization, the $Cu_{2-x}Se$ NSs were precipitated with ethanol and collected by centrifugation at 3,500 r.p.m. for 3 min and cleaned by repeated precipitation with acetone and redispersion in $CHCl_3$ for three times until the supernatant becomes clear. The final $Cu_{2-x}Se$ NSs were dispersed in toluene and stored in a nitrogen filled glovebox.

Synthesis of Cu_2GeSe_3 (CGSe) and $Cu_2GeS_xSe_{3-x}$ (CGSSe) NSs:

For the synthesis of CGSe NSs, the aforementioned mixture containing $Cu_{2-x}Se$ NSs (i.e. solution 1) were cooled to room temperature and 0.2 mmol GeI_4 was added. The mixture was sealed and heated to 100 °C under vacuum for 2 mins. After filled with nitrogen, the mixture was heated to 210 °C, and kept at this temperature for 2 h before cooled down to room temperature. The product was purified using the same procedure as for initial Cu_2Se NSs.

For the synthesis of CGSSe NSs, all the experimental conditions were kept the same as those for the synthesis of CGSe NSs, except the final temperature was kept as 250 °C for 2 h.

Synthesis of $Cu_2ZnGeSe_4$ (CZGSe) NSs:

For the synthesis of CZGSe NSs, the aforementioned mixture containing Cu_2Se NSs (i.e. solution 1) were cooled to room temperature and 0.2 mmol GeI_4 was added. The mixture was sealed and heated to 100 °C under vacuum for 2 min. After filled with nitrogen, the mixture was heated to 210 °C. At 210 °C, 0.4 mmol $ZnCl_2$ dissolved in 1 mL OAm at 100 °C was injected into the mixture. The reaction mixture was kept at 210 °C for 2 h before cooled down to room temperature. The product was purified using the same procedure as for initial $Cu_{2-x}Se$ NSs.

Synthesis of $Cu_2ZnGeS_xSe_{4-x}$ (CZGSSe) NSs:

For the synthesis of CZGSe NSs, the aforementioned mixture containing Cu_2Se NSs (i.e. solution 1) were cooled to room temperature and 0.2 mmol GeI_4 was added. The mixture was sealed and heated to 100 °C under vacuum for 2 min. After filled with nitrogen, the mixture was heated to 250 °C. At 250 °C, 0.4 mmol $ZnCl_2$ dissolved in 1 mL OAm at 100 °C was injected into the mixture. The reaction mixture was kept at

250 °C for 2 h before cooled down to room temperature. The product was purified using the same procedure as for initial $Cu_{2-x}Se$ NSs.

Characterization:

X-Ray Diffraction (XRD). X-ray diffraction patterns were obtained by using a Rigaku MiniFlex 600 diffractometer, equipped with a Cu Kα X-ray source (λ=1.5418 Å). Samples for XRD analysis were prepared by depositing the purified NSs dispersed in toluene on a glass substrate.

Transmission Electron Microscopy (TEM): TEM, High-resolution TEM (HRTEM) images, selected area electron diffraction (SAED) patterns, STEM Energy Dispersive X-ray Spectroscopy (EDS) mapping were performed on a Hitachi HF-3300 microscope operating at 300 kV. TEM Samples were prepared by dropping the diluted colloidal nanosheets onto carbon coated 200 mesh nickel grids.

Atomic force microscopy (AFM) images were recorded in a non-contact mode using a model PSIA Xe-150 (Park System).

UV-vis-NIR Spectroscopy. Absorbance spectra of nanocrystals dissolved in toluene were measured in 1 cm path length quartz cuvettes using a Cary 5000 UV-vis-NIR (Agilent Technologies) spectrophotometer.

X-ray Photoelectron Spectroscopy (XPS). XPS data were collected with a MultiLab ESCA 2000 spectrometer equipped with a monochromatic Al Kα X-ray source and a concentric hemispherical analyzer.

Raman Spectroscopy. Raman spectroscopy analysis was performed with a confocal microprobe Raman system (Thermo Nicolet Almega XR Raman Microscope) with an exciting wavelength of 532 nm. Colloidal nanocrystals were drop-cast on a silicon wafer in air.

3. Results and Discussion

In the first step of the synthesis, $Cu_{2-x}Se$ NSs were prepared by injecting Se-precursor into a hot solution of CuI in oleylamine/oleic acid mixture. As shown in Fig. 2a, the obtained $Cu_{2-x}Se$ has triangular 2D sheet like morphology with lateral size in micrometers. Besides these triangular sheets, a small portion of nanoparticles were also present in the final product, which were removed by slow centrifugation. A closer look at the NSs (Fig. 2b) revealed that the NSs are decorated with smaller particles of size 6-8 nm. The SAED pattern (inset in Fig. 2b) of the nanosheet consists of ring and bright spot patterns correspond to poly and single crystalline nature, respectively. HRTEM images recorded at two different places near the edge show differently oriented lattice fringes (Fig. S1a), as well as continuous lattice fringes (Fig. S1b). The observed interplanar distance (0.201 nm) corresponds to (220) plane of cubic $Cu_{2-x}Se$. This suggests that the spot patterns should have originated from the single crystalline nanosheet template and the ring pattern is due to differently oriented nanoparticles on the NSs. The crystal structure of the NSs was studied by X-ray diffraction (XRD) analysis. It was found that the NSs are composed of cubic $Cu_{2-x}Se$ and hexagonal CuSe crystal phases with majority of the peaks match with cubic $Cu_{2-x}Se$ (Fig. 2c). The importance of the CuSe secondary phase in the nanosheet formation will be discussed later. The energy-dispersive X-ray spectroscopy (EDS) analysis showed a stoichiometry of $Cu_{1.1}Se$ for the NSs (Fig. 2d). This is due to the presence of both the $Cu_{2-x}Se$ and CuSe phases in the NSs.

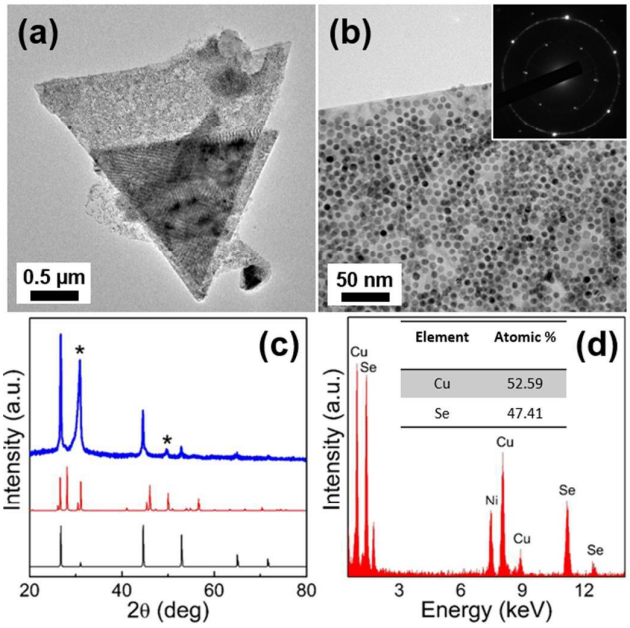

Fig. 2 (a, b) TEM images (c) XRD pattern and (d) EDS spectrum of $Cu_{2-x}Se$ NSs synthesized at 150 °C for 2h. Inset in b shows the SAED pattern of the NS. The reference diffraction patterns of cubic $Cu_{2-x}Se$ (Black) and hexagonal CuSe (Red) are shown in c. The diffraction peaks marked by (*) are correspond to CuSe.

To gain more information on the formation mechanism of NSs, a series of controlled experiments were carried out. First we studied the nanosheet formation as a function of reaction time. As shown in the XRD patterns in Fig. S2, pure cubic $Cu_{2-x}Se$ phase was observed when the reaction was stopped immediately after Se-precursor injection. Hexagonal CuSe phase appeared after 30 mins reaction time and remained as a secondary phase even after 2 h. Further increasing the reaction time to 6 h, intensity of CuSe phase decreased and $Cu_{2-x}Se$ phase became dominant. Fig. 3 shows the TEM images at different reaction times. Pure $Cu_{2-x}Se$ phase obtained at 0 min appeared as spherical nanoparticles of size less than 10 nm (Fig. 3a). EDS measurements show a Cu:Se ratio of 1.9:1 for the nanoparticles (Fig. S3a). This is in accordance with the XRD observation of pure $Cu_{2-x}Se$ phase. After 30 and 60 min reaction time, 2D nanoparticle assemblies (Fig. 3b and c) were observed and the EDS spectrum (Fig. S3b) show a stoichiometry of Cu:Se ratio of 1.3:1 for the NSs obtained after 30 min. This shows that an increase in the oxidation number for copper ions. These observations together with XRD analysis show that longer reaction time leads to the partial oxidation of Cu^{+} ions to Cu^{2+} ions and result in the secondary CuSe phase

formation. However, we were not able to identify and isolate the CuSe phase in the nanostructures. We believe that both $Cu_{2-x}Se$ and CuSe phase co-exist in the nanoparticle assembly. Further increasing the reaction time to 6 h, the nanocrystals are recrystallized to form nearly single-crystalline NSs. SAED patterns in the insets of Fig. 3a-d clearly show a gradual transition from polycrystalline nanoparticles to single-crystalline NSs.

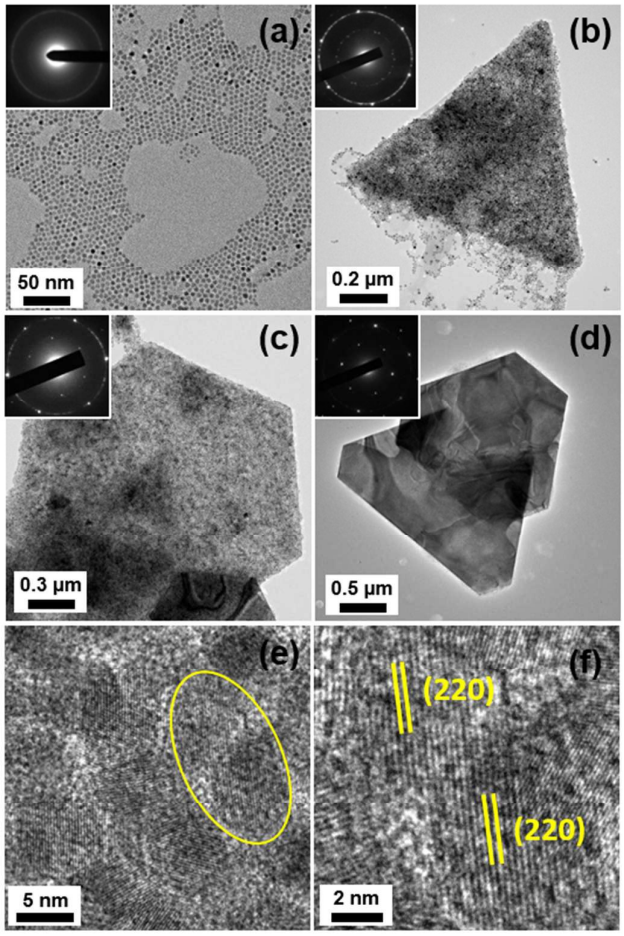

Fig. 3 TEM images of $Cu_{2-x}Se$ NSs synthesized at different reaction times. (a) 0 min, (b) 30 min, (c) 1 h and (d) 6 h. Top left insets in each image show the corresponding SAED patterns. (e) HRTEM image of the nanoparticle assembly obtained after 60 min. (f) Magnified HRTEM image of the marked portion in (e).

HRTEM image obtained from the NSs formed after 60 min, show two fused nanoparticle with continuous lattice fringes (Fig. 3f). This suggests an oriented attachment in the nanoparticle assemblies. CuSe has a hexagonal crystal structure (P63/mmc space group) with intrinsic anisotropic character to grow in 2D morphology.[39] Cubic $Cu_{2-x}Se$ has a FCC crystal structure and the surface energy of the planes in FCC structure follow the order: (110) > (100) > (111). Since the initially formed primary $Cu_{2-x}Se$ NCs have very high surface energy (110) planes, there is a strong driving force for the nanoparticles to assemble and oriented attach to decrease the surface energy and become stable at higher temperatures.[37,38] Hence, we attribute the 2D nanocrystal assembly formation to the synergetic effect of the *in situ* oxidation of Cu^{+} to Cu^{2+} ions and presence of high surface energy planes in cubic $Cu_{2-x}Se$ nanoparticles. The entire process is depicted in Fig. 4.

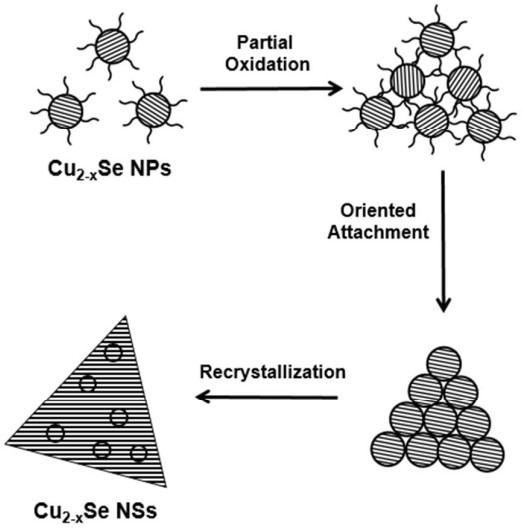

Fig. 4 Schematic illustration of the formation mechanism of $Cu_{2-x}Se$ nanosheets.

In the next step, we tried to find out the source for the oxidation of Cu^{+} ions. After carefully examining all the reaction parameters, we found that the Se-precursor preparation method is the main reason for the oxidation of Cu^{+} ions in the reaction mixture. In our method, the Se-precursor was prepared by dissolving Se powder in a mixture of OAm and 1-DDT in air. We used technical OAm, which is only 70% pure and contains water in it. It is well known that Cu^{+} ions are prone to oxidize in the presence of moisture or air.[40] When Se-precursor is prepared using technical oleylamine, it is reasonable to expect it to act as oxidizing agent for the Cu^{+} ions. To verify this fact, we prepared Se-precursor using dried OAm under air free condition (vacuum at 80 °C for 1 h). When this precursor was used for the synthesis, only nanoparticles morphology was observed after 2 h reaction at 150 °C (Fig. S4a-b). The XRD pattern showed the presence of single $Cu_{2-x}Se$ phase without any CuSe secondary phase (Fig. S4c). This was further supported by EDS analysis which gave a stoichiometry of $Cu_{1.8}Se$ (Fig. S4d). In another set of experiments we changed the molar ratios of Cu^{+} ion to Se powder, since the oxidation rate can be affected by the availability of Cu^{+} ions. As the expected, when the Cu^{+} concentration was decreased (Cu:Se-0.66:1), all the Cu^{+} ions were oxidized and phase pure hexagonal CuSe NSs were obtained (Fig. S5a and b). When excess of Cu^{+} ions were present (Cu:Se-2:1), the water content in the precursor is not enough to produce significant oxidation and only cubic $Cu_{2-x}Se$ nanoparticles were produced (Fig. S5d).

These observations clearly proves that in situ oxidation of Cu^+ ions to form CuSe secondary phase is the driving force for formation of $Cu_{2-x}Se$ NSs.

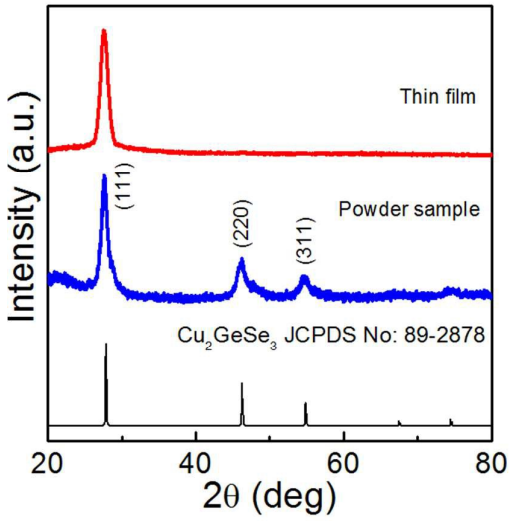

Fig. 5 XRD patterns of powder and thin film of CGSe NSs obtained from $Cu_{2-x}Se$ NSs *via* partial cation exchange.

Since 2D ternary and quaternary chalcogenide NSs are our prime interest, we carried out Ge^{4+} cation exchange in $Cu_{2-x}Se$ NSs. CGSe NSs were formed after reacting the $Cu_{2-x}Se$ NSs with Ge^{4+} precursor (i.e., GeI_4) at 210 °C for 2 h. The presence of 1-DDT and OAm in the reaction mixture facilitate the solubilization of germanium salt via formation of metal-OAm and metal-DDT complexes. This helps to react with the $Cu_{2-x}Se$ nanosheets in a homogeneous way. XRD analysis from Fig. 5 confirmed that the CGSe nanosheet has a cubic structure with F-43m space group (JCPDS No. 89-2878). For the drop casted thin films, significant preferred orientation along (111) plane is observed, which confirms that the samples are consist of only nanosheet morphology. The composition of the as-synthesized CGSe NSs was characterized by EDS analysis (Fig. S6a), which showed a Cu/Ge/Se/S atomic ratio of 1.95/1.00/3.10/0.35, which corresponds to a stoichiometry of Cu_2GeSe_3. The higher reaction temperature was found to be necessary for the formation of phase pure CGSe NSs. Fig. S7 shows the XRD patterns of the partial CE reaction products at different reaction temperatures. When the CE was performed at 150 °C for 2 h, no reaction took place and only $Cu_{2-x}Se$ phase was observed. CGSe phase started to appear at 180 °C, and phase pure CGSe was obtained at 210 °C. The necessity of higher reaction temperature may due to the lower ion mobility of Ge^{4+} relative to that of Cu^+ within the anionic framework.

In literature, most of the partial cation exchange reactions were carried out at low temperature in the presence of a soft base such as tri-n-octylphosphine (TOP).[22,27-29] TOP can selectively bind to the Cu^+ ions (soft acid) and helps in extracting Cu^+ from $Cu_{2-x}Se$ nanocrystals. However, when TOP was used in our method, the nanosheet morphology was collapsed. This may be due to the fast extraction rate of Cu^+ ions than the insertion of Ge^{4+} ions in $Cu_{2-x}Se$ NSs. Hence we adopted higher reaction temperatures instead of using TOP. Even though higher CE reaction temperatures were used, we did not observe any secondary phase (i.e., $GeSe_2$) formation. This can be easily understood by the topotactic nature of the most cation CE reactions, in which the crystal structure of the parent nanocrystal is preserved in the product.[29,41,42] In our method the CE reaction stopped after reaching final composition of Cu_2GeSe_3. Cu_2GeSe_3 has a cubic crystal structure same as $Cu_{2-x}Se$, whereas $GeSe_2$ has a layered structure in which Se-Ge-Se layers stacked together *via* van der Waals interaction.[43] The formation of $GeSe_2$ would require much higher energy for the reorganization of anionic lattice as well as effective Cu^+ ion extracting agents such as TOP.

It is well known that the band gap of metal chalcogenide nanostructures can be easily tuned by alloying two chalcogens. A best example is the selenization process of Cu_2ZnSnS_4 (CZTS) thin films, which alters the band gap and improve the

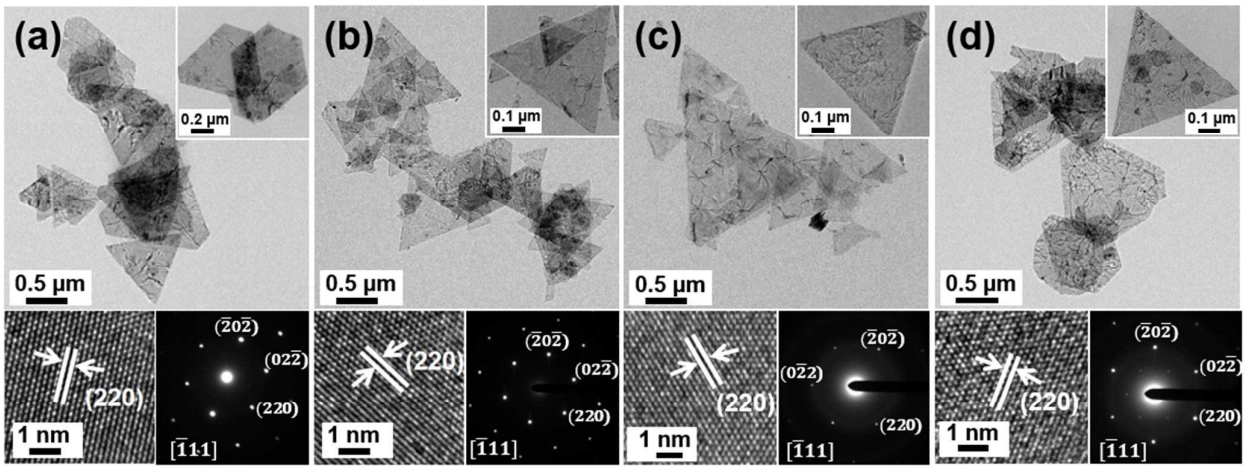

Fig. 6 TEM and HRTEM images and SAED pattern of (a) CGSe, (b) CGSSe, (c) CZGSe, and (d) CZGSSe nanosheets.

performance of CZTS thin film solar cells. In our method, we could easily alloy sulfur with CGSe NSs by increasing the CE reaction temperature to 250 °C. At higher temperatures, the 1-DDT molecules present in the reaction mixture can decompose and incorporate sulfur into the CGS NSs, which gives a composition of $Cu_2GeS_xSe_{3-x}$ (CGSSe). EDS spectra in Fig. S6b, shows Cu/Ge/S/Se atomic ratio of 2.04/1.00/1.45/1.67 for $Cu_2GeS_xSe_{3-x}$ NSs, which is a clear indication of the alloying of S in CGSe NSs. It should be noted that, it is not possible to precisely control the S content in the NSs, since the incorporation of S occurs due to the decomposition of 1-DDT ligands. Impressively, our CE method can be extended to synthesize quaternary $Cu_2ZnGeSe_4$ (CZGSe) and alloyed $Cu_2ZnGeS_xSe_{4-x}$ (CZGSSe) NSs by adding $ZnCl_2$ dissolved in OAm at 210 and 250 °C, respectively (Fig. S6c and d). As shown in Fig. S8, the powder XRD pattern of CGSe and CGSSe NSs match well with that of the standard cubic CGSe (JCPDS no. 89-2878). Whereas, the XRD patterns of CZGSe and CZGSSe NSs match well with that of the tetragonal-symmetry structure with the I-42m space group (JCPDS no. 52-0867). For the S alloyed samples, the (111) peak is shifted to higher angles, which is an indication of decreased lattice constants arising from the substitution of smaller S^{2-} to the larger Se^{2-} in lattices (Fig. S8c).

Fig. 6a-d shows the typical transmission electron microscopy (TEM) images of the CGSe, CGSSe, CZGSe and CZGSSe NSs, respectively. In contrast to the starting $Cu_{2-x}Se$ NSs, the CE synthesized ternary and quaternary chalcogenides show clear 2D nanosheet morphology without any particles. This is due to the relatively higher CE reaction temperatures (210 and 250 °C), which crystallizes the nanoparticles into NSs. Shape and size of the NSs are not uniform and most of the NSs are triangular in shape with an average lateral size of 0.5-1.5 µm. The NSs are thin (3~5 nm) as deduced from the AFM analysis (Fig. S9). The observed interplanar distances from the high resolution TEM (HRTEM) images are about 0.19 nm, which is in accordance with the (220) plane of the cubic structure. The selected area electron diffraction (SAED) patterns from the individual NSs show a spot pattern that is an indication of the single-crystalline nature of these NSs. We used EDS elemental mapping to analyze the elemental distribution of the CZGSSe alloyed NSs. As shown in Fig. S10, Cu, Zn, Ge, S and Se atoms distributed homogeneously in the CZGSSe NSs and no noticeable nano-heterostructure can be observed in the mapping. Further, we analyzed the oxidation states of all the components in CZGSSe NSs using XPS (Fig. S11). The binding energies clearly show that copper is present as Cu^+, zinc as Zn^{2+}, germanium as Ge^{4+}, sulfur as S^{2-} and selenium as Se^{2-}. Raman spectroscopy was employed to analyze the phase purity of the ternary and quaternary chalcogenide NSs. As shown in Fig. S12, the Raman spectrum of $Cu_{2-x}Se$ has a major peak at 265 cm^{-1} due to the Se-Se stretch vibration of the Se^{2-} ions, which is clearly absent in the ternary and quaternary NSs. This indicates the complete transformation of $Cu_{2-x}Se$ into ternary and quaternary chalcogenide NSs. The CGSe and CGSSe NSs have a major peak at 202 cm^{-1}, whereas CZGSe and CZGSSe NSs has a major peak at 204 cm^{-1}. The observed peak at 204 cm^{-1} is in good agreement with the reported A1 mode.[44] No other impurity peaks were observed in the Raman spectra.

The optical properties of the NSs and NPs were studied by measuring UV-vis-NIR absorption spectra. As shown in Fig. 7a, $Cu_{2-x}Se$ NSs exhibit a broad localized surface plasmon resonance in the NIR region. This peak is suppressed by incorporation of Ge^{4+} and Zn^{2+} into the $Cu_{2-x}Se$ NSs. Ternary and quaternary NSs have absorption onset around 1200-1300 nm, suggesting their narrow bandgap. The band-gap energies of these NSs were determined by extrapolating the linear regions of the plots of $(\alpha hv)^2$ versus photon energy (hv). S alloying and Zn^{2+} incorporation resulted in band gap tuning from 1 to 1.25 eV CGSe NSs (Fig. 7b). These values fall in the range of optimum band gap for the light absorbers in thin film solar cells.

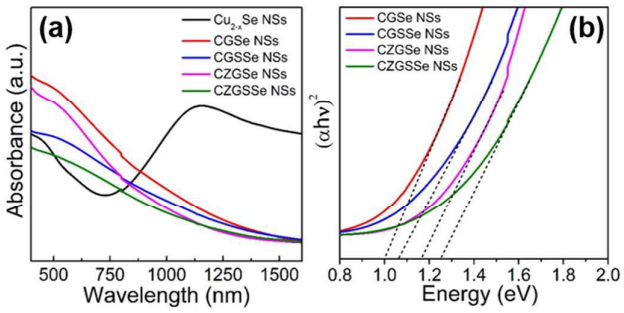

Fig. 7 (a) UV-vis-NIR absorption spectra of $Cu_{2-x}Se$ CGSe, CGSSe, CZGSe and CZGSSe NSs. (b) Plots of $(\alpha hv)^2$ versus energy with an extrapolation of the spectra (dashed lines) to determine optical band gap values of NSs.

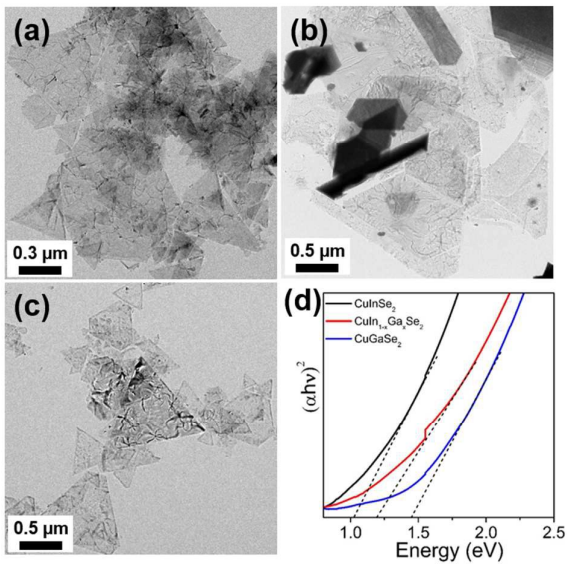

Fig. 8 TEM images of (a) $CuInSe_2$ (b) $CuIn_{1-x}Ga_xSe_2$ and (c) $CuGaSe_2$ NSs. (d) calculated bandgap values of $CuInSe_2$, $CuIn_{1-x}Ga_xSe_2$ and $CuGaSe_2$ NSs.

To demonstrate the generality of our method, we also carried out partial CE reactions to produce $CuIn_{1-x}Ga_xSe_2$ NSs (x = 0, 0.5 and 1) from $Cu_{2-x}Se$ NSs. $CuIn_{1-x}Ga_xSe_2$ NSs were prepared using the same method for CGSe nanosheets except GeI_4 was replaced with 0.2 mmol $InCl_3$ for $CuInSe_2$, mixture of 0.1 mmol $InCl_3$ and 0.1 mmol $GaCl_3$ for $CuIn_{0.5}Ga_{0.5}Se_2$ and 0.2 mmol $GaCl_3$ for $CuGaSe_2$ NSs. Fig. S13 shows the XRD patterns of the obtained NSs. $CuInSe_2$ NSs have a tetragonal-symmetry structure with the I-42m space group (JCPDS no. 40-1487). Upon addition of gallium, the (111) peak of $CuInSe_2$ shifted to higher angles due to substitution of smaller Ga^{3+} to the larger In^{3+} ions. As shown in the TEM images (Fig. 8a-c), all the samples have clear 2D nanosheet morphology. The bandgap values are changed from 1.02 to 1.44 eV upon Ga^{3+} addition (Fig. 8d).

In summary, we have detailed a synthetic procedure to produce copper based ternary and quaternary alloyed chalcogenide NSs using $Cu_{2-x}Se$ NSs as templates. The Se-precursor preparation method directs the final morphology of the template $Cu_{2-x}Se$ NSs. When Se-precursor was prepared in air using technical oleylamine, Cu^+ ions in the reaction mixture are partly oxidized to form CuSe secondary phase which drives the formation of $Cu_{2-x}Se$ NSs. Partial CE of Cu^+ ions with Ge^{4+} and Zn^{2+} ions produced micrometer sized thin CGSe and CZGSe NSs. By increasing CE reaction temperature, it is possible to alloy S with CGSe and CZGSe nanostructures, which resulted in the increased band gap of these materials. Our preliminary studies showed that this method can also be extended to synthesis other ternary NSs such as $CuIn_{1-x}Ga_xSe_2$. Future work will focus on the utilization of these single-crystalline nanosheets for the optoelectronic applications.

Acknowledgements

This work was supported by the DGIST R&D Program of the Ministry of Science, ICT and Future Planning (15-BD-0401) and the Ministry of Education (MOE) and National Research Foundation of Korea (NRF) through the Human Resource Training Project for Regional Innovation (No. 2015035858).
J. Kim is grateful for financial support by the Priority Research Center Program (2015R1D1A1A09060653) through the National Research Foundation of Korea (NRF).

Notes and references

1 Q. H. Wang, K. Kalantar-Zadeh, A. Kis, J. N. Coleman and M. S. Strano, *Nat Nanotech.*, 2012, **7**, 699.
2 S. Z. Butler, S. M. Hollen, L. Cao, Y. Cui, J. A. Gupta, H. R. Gutiérrez, T. F. Heinz, S. S. Hong, J. Huang, A. F. Ismach, E. Johnston-Halperin, M. Kuno, V. V. Plashnitsa, R. D. Robinson, R. S. Ruoff, S. Salahuddin, J. Shan, L. Shi, M. G. Spencer, M. Terrones, W. Windl and J. E. Goldberger, *ACS Nano*, 2013, **7**, 2898.
3 M. Xu, T. Liang, M. Shi and H. Chen, *Chem. Rev.*, 2013, **113**, 3766.
4 X. Huang, C. Tan, Z. Yin and H. Zhang, *Adv. Mater.*, 2014, **26**, 2185.
5 D. Jariwala, V. K. Sangwan, L. J. Lauhon, T. J. Marks and M. C. Hersam, *ACS Nano*, 2014, **8**, 1102.
6 G. Eda and S. A. Maier, *ACS Nano*, 2013, **7**, 5660.
7 M. Bernardi, M. Palummo and J. C. Grossman, *Nano Lett.*, 2013, **13**, 3664.
8 D. Aldakov, A. Lefrancois and P. Reiss, *J. Mater. Chem. C*, 2013, **1**, 3756.
9 F.-J. Fan, L. Wu and S.-H. Yu, *Energy Environ. Sci.*, 2014, **7**, 190.
10 S. C. Riha, B. A. Parkinson and A. L. Prieto, *J. Am. Chem. Soc.*, 2011, **133**, 15272.
11 C. Yang, B. Zhou, S. Miao, C. Yang, B. Cai, W.-H. Zhang and X. Xu, *J. Am. Chem. Soc.*, 2013, **135**, 5958.
12 J.-j. Wang, P. Liu, C. C. Seaton and K. M. Ryan, *J. Am. Chem. Soc.*, 2014, **136**, 7954.
13 P. Ramasamy and J. Kim, *Chem. Asian J.*, 2015, **10**, 1468.
14 C. J. Hages, S. Levcenco, C. K. Miskin, J. H. Alsmeier, D. Abou-Ras, R. G. Wilks, M. Bär, T. Unold and R. Agrawal, *Prog. Photovolt: Res. Appl.*, 2015, **23**, 376.
15 M. Ibáñez, R. Zamani, A. LaLonde, D. Cadavid, W. Li, A. Shavel, J. Arbiol, J. R. Morante, S. Gorsse, G. J. Snyder and A. Cabot, *J. Am. Chem. Soc.*, 2012, **134**, 4060.
16 M. Ibáñez, R. Zamani, W. Li, D. Cadavid, S. Gorsse, N. A. Katcho, A. Shavel, A. M. López, J. R. Morante, J. Arbiol and A. Cabot, *Chem. Mater.*, 2012, **24**, 4615.
17 F.-J. Fan, Y.-X. Wang, X.-J. Liu, L. Wu and S.-H. Yu, *Adv. Mater.*, 2012, **24**, 6158.
18 J. van Embden, A. S. R. Chesman and J. J. Jasieniak, *Chem. Mater.*, 2015, **27**, 2246.
19 A. Singh, H. Geaney, F. Laffir and K. M. Ryan, *J. Am. Chem. Soc.*, 2012, **134**, 2910.
20 A. Singh, C. Coughlan, F. Laffir and K. M. Ryan, *ACS Nano*, 2012, **6**, 6977.
21 X.-J. Wu, X. Huang, X. Qi, H. Li, B. Li and H. Zhang, *Angew. Chem.,* 2014, **126**, 9075.
22 V. Lesnyak, C. George, A. Genovese, M. Prato, A. Casu, S. Ayyappan, A. Scarpellini and L. Manna, *ACS Nano*, 2014, **8**, 8407.
23 L. Mu, F. Wang, B. Sadtler, R. A. Loomis and W. E. Buhro, *ACS Nano*, 2015, **9**, 7419.
24 L. Shi and Q. Li, *CrystEngComm*, 2011, **13**, 6507.
25 J. Park and S.-W. Kim, *J. Mater. Chem.*, 2011, **21**, 3745.
26 L. De Trizio, M. Prato, A. Genovese, A. Casu, M. Povia, R. Simonutti, M. J. P. Alcocer, C. D'Andrea, F. Tassone and L. Manna, *Chem. Mater.*, 2012, **24**, 2400.
27 W. van der Stam, A. C. Berends, F. T. Rabouw, T. Willhammar, X. Ke, J. D. Meeldijk, S. Bals and C. de Mello Donega, *Chem. Mater.*, 2015, **27**, 621.
28 Q. A. Akkerman, A. Genovese, C. George, M. Prato, I. Moreels, A. Casu, S. Marras, A. Curcio, A. Scarpellini, T. Pellegrino, L. Manna and V. Lesnyak, *ACS Nano*, 2015, **9**, 521.
29 W. van der Stam, E. Bladt, F. T. Rabouw, S. Bals and C. de Mello Donega, *ACS Nano*, 2015, **9**, 11430.
30 H. Zhou, W.-C. Hsu, H.-S. Duan, B. Bob, W. Yang, T.-B. Song, C.-J. Hsu and Y. Yang, *Energy Environ. Sci.*, 2013, **6**, 2822.
31 D. B. Mitzi, O. Gunawan, T. K. Todorov, K. Wang and S. Guha, *Sol. Energy Mater. Sol. Cells*, 2011, **95**, 1421.
32 G. Marcano and L. Nieves, *J. Appl. Phys.*, 2000, **87**, 1284.
33 D. M. Schleich and A. Wold, *Mater. Res. Bull.*, 1977, **12**, 111.
34 H. Matsushita, T. Ichikawa, and A. Katsui, *J. Mater. Sci.* 2005**, 40**, 2003.
35 L. Shi and P. Yin, *Dalton Trans.*, 2013, **42**, 13607.
36 Y. Liu, D. Yao, L. Shen, H. Zhang, X. Zhang and B. Yang, *J. Am. Chem. Soc.*, 2012, **134**, 7207.
37 M. P. Boneschanscher, W. H. Evers, J. J. Geuchies, T. Altantzis, B. Goris, F. T. Rabouw, S. A. P. van Rossum, H. S. J. van der Zant, L. D. A. Siebbeles, G. Van Tendeloo, I. Swart, J.

Hilhorst, A. V. Petukhov, S. Bals and D. Vanmaekelbergh, *Science*, 2014, **344**, 1377.
38 G. S. Shanker, A. Swarnkar, A. Chatterjee, S. Chakraborty, M. Phukan, N. Parveen, K. Biswas and A. Nag, *Nanoscale*, 2015, **7**, 9204.
39 Y.-Q. Liu, F.-X. Wang, Y. Xiao, H.-D. Peng, H.-J. Zhong, Z.-H. Liu and G.-B. Pan, *Sci. Rep.*, 2014, **4**, 5998.
40 S. C. Riha, D. C. Johnson and A. L. Prieto, *J. Am. Chem. Soc.*, 2011, **133**, 1383.
41 J. B. Rivest and P. K. Jain, *Chem. Soc. Rev.*, 2013, **42**, 89.
42 B. J. Beberwyck, Y. Surendranath and A. P. Alivisatos, *J. Phys. Chem. C*, 2013, **117**, 19759.
43 B. Mukherjee, Z. Hu, M. Zheng, Y. Cai, Y. P. Feng, E. S. Tok and C. H. Sow, *J. Mater. Chem.*, 2012, **22**, 24882.
44 M. Guc, S. Levcenko, V. Izquierdo-Roca, X. Fontané, E. Arushanov and A. Pérez-Rodríguez, *J. Appl. Phys*., 2013, **114**, 193514.